Structural and Multidisciplinary Optimization
https://doi.org/10.1007/s00158-018-2033-0

RESEARCH PAPER

Seismic energy dissipation-based optimum design of tuned mass dampers

Mohammad Reza Shayesteh Bilondi[1] · Hessam Yazdani[2] · Mohsen Khatibinia[1]

Received: 10 April 2018 / Revised: 9 June 2018 / Accepted: 14 June 2018

Abstract

Tuned mass dampers (TMDs) are a subclass of dynamic vibration absorbers that consist of a mass-spring-damper unit that is attached to a structure to adjust its response to seismic and wind loads. The efficacy, performance and optimum design of a TMD strongly depend not only on its mass, stiffness and damping as well as the input energy and the structure characteristics, but also on the structural response parameter(s) that the TMD is intended to mitigate. In that respect, this study evaluates the suitability of four objective functions for the optimum design of the TMD of an inelastic, steel moment-resisting frame (SMRF) under an artificial, white-noise excitation. The objective functions include 1) the maximum roof lateral displacement, 2) the maximum drift, 3) the root mean square of drifts and 4) the cumulative hysteretic energy of the SMRF. The results indicate that the SMRF equipped with a TMD optimized using the cumulative hysteretic energy of the SMRF as the objective function exhibits the best seismic response under the artificial earthquake. Further examining the response of the TMD-equipped SMRF under four historic earthquake records shows that equipping a structure with a TMD optimized using an artificial earthquake will not warrant that the structure will exhibit a better seismic performance in all measures compared with when no TMD is used. Put other way, while the minimization of cumulative hysteretic energy could be the best objective function for a case subjected to an artificial earthquake, under real earthquakes, none of the objective functions consistently results in a better seismic performance. This behavior is attributed to detuning effects arising from major structural damages and significant period shifts that occur during strong earthquakes.

Keywords Earthquake protective systems · Viscoelastic damper · Dynamic vibration absorbers · Metaheuristic optimization algorithms

1 Introduction

Tuned mass dampers (TMDs) are a subclass of dynamic vibration absorbers that consist of a mass that is attached to the structure through a parallel spring-viscous damper unit. Under dynamic loading, the mass moves relative to the structure and attenuates its kinetic energy. Examples of structures equipped with a TMD include the Citigroup Center in New York (279 m high), the Burj Al Arab in Dubai (280 m high), the Yokohama Landmark Tower in Yokohama (296.3 m high), the Taipei 101 in Taipei (509.2 m high) and the CN Tower in Toronto (553.3 m high).

TMDs were originally introduced to control the wind vibrations of elastic structures. Their application for the mitigation of seismic effect, in contrast, has proven challenging because various modes of vibration require different tunings and also detuning may occur if the structure dynamics enters into the nonlinear régime (Saaed et al. 2015). This challenge has sparked growing research interest in studying and particularly optimizing the damping and the frequency ratio tuning of TMDs for seismic mitigation applications.

Den Hartog (1956) was the first to develop closed-form expressions for the optimum parameters of undamped single-degree-of-freedom (SDOF) main systems subjected to a harmonic excitation. In studying the influence of a group of selected elastoplastic vibration absorbers in the response of linear SDOF systems subjected to an earthquake excitation, Gupta and Chandrasekaren (1969) found

Responsible Editor: Nestor V. Queipo

✉ Mohsen Khatibinia
m.khatibinia@birjand.ac.ir

[1] Department of Civil Engineering, University of Birjand, Birjand, Iran

[2] Department of Civil and Environmental Engineering, Howard University, Washington, DC, USA

Published online: 22 June 2018

that the impact of the vibration absorbers was only minimal and concluded that they are not as effective for earthquake excitations as they are for sinusoidal ones. Wirsching and Yao (1973) modeled the dynamic behavior of multistory structures with an absorber attached to the roof, a nonlinear spring between the foundation and structure and a damping mechanism at the first floor. They observed a considerable reduction in the peak relative response of the top floors by using vibration absorbers with a damping ratio of 20%. Wirsching and Campbell (1973) calculated the optimum values for vibration absorbers' parameters and demonstrated their effectiveness in reducing the first mode response of five- and 10-storey linear structures under a Gaussian white-noise base acceleration even with relatively small values of the absorber mass. Warburton (1982) extended the work of Den Hartog (1956) and derived expressions for the optimum absorber parameters of undamped SDOF systems under harmonic and white-noise random excitations. Such dynamic systems, however, are not equivalent to systems excited at the base by ground accelerations, and therefore their optimum values are not applicable for earthquake loads. Villaverde (1985) showed that the attachment of a small heavily-damped system in resonance can increase the damping of a building, thus reducing its response to earthquake excitations. Sadek et al. (1997) derived the optimum frequency (tuning) and damping ratios of the TMD of SDOF and MDOF systems under different earthquake excitations with emphasis on achieving an equal and large modal damping in their first two modes of vibration (MDOF: multiple-degree-of-freedom). Rana and Soong (1998) investigated the influence of the detuning of a TMD's parameters on its performance using steady-state harmonic excitation and time-history analyses. They first showed that each mode of an MDOF structure can be represented by a particular SDOF structure and then used this toward controlling different modes of a multimodal structure using multituned mass dampers.

An active area of research is the optimization of passive and active vibration control systems in tall buildings equipped with such systems (Aldwaik and Adeli 2014). For instance, Bakre and Jangid (2007) used nonlinear programming to obtain the optimum parameters of a TMD system attached to a viscously-damped SDOF main system for various combinations of excitation and response parameters such as relative displacement, velocity of main mass and force transmitted to the support. They also derived explicit formulae for the TMD system's damping and tuning frequency and the corresponding minimized response. Traditional techniques of this kind, however, are not suitable for the optimization of TMD-equipped systems (e.g. towers) because they are typically large/tall and expected to exhibit a complex seismic response. This conundrum has sparked research on the optimization of the design and location(s) of TMDs in different types of structures using metaheuristic optimization algorithms. Some of these studies are outlined below.

Singh et al. (2002) used the genetic algorithm (GA) to optimize the TMD design for controlling the torsional response of building systems subjected to bidirectional seismic inputs. Singh and Moreschi (2002) employed GA for the optimum, seismic, performance-based design of TMD-equipped structures. Desu et al. (2006) used GA to optimally design a TMD to control coupled lateral and torsional vibrations of asymmetric buildings. The particle swarm optimization (PSO) has also been employed for the optimum design of TMD systems. Leung et al. (2008) and Leung and Zhang (2009) used PSO to find the optimum mass ratio, damping and tuning frequency of TMDs attached to viscously-damped SDOF main systems. The multi-objective PSO algorithm was used by Khatibinia et al. (2016) to optimize TMD parameters considering soil-structure interactions. Bekdaş and Nigdeli (2011) and (Nigdeli et al. 2017) optimized TMDs subjected to harmonic loading and ground acceleration using the harmony search (HS) algorithm. Using HS, Nigdeli and Bekdas (2013) calibrated TMDs for preventing brittle fracture of reinforced concrete buildings. An improved HS was used by Zhang and Zhang (2017) to find optimum TMD parameters for high-rise intake towers. Examples of other algorithms that have been used for the optimization of TMDs and TMD-equipped systems include the ant colony algorithm (Farshidianfar and Soheili 2013), the charged system search (Kamgar et al. 2017; Shahrouzi et al. 2017), the grey wolf optimizer (Kamgar et al. 2017), the gravitational search algorithm (Khatibinia et al. 2017), the bat algorithm (Bekdaş and Nigdeli 2017; Bekdaş et al. 2018) and the differential evolution algorithm (Lu et al. 2018), among others.

The studies surveyed above assumed an elastic behavior for the structure. The inelastic behavior of structures, however, has proven to considerably influence the efficacy of TMDs and their optimum design. For instance, Wong (2008) showed that TMDs are mostly effective in structures that yield at large displacements, which in turn allow storing larger amounts of energy inside the TMD and releasing it later in the form of damping energy when the response is not at a critical state. In addition, the inelastic behavior of the structure would require TMD performance indices different from those used for elastic structures. For example, Mohebbi and Joghataie (2012) considered reduction in total structural drift and cumulative hysteretic energy (plastic energy) as performance indices for a TMD-equipped, eight-story, nonlinear building with bilinear hysteretic material behavior and subjected to a white-noise excitation.

Further research is required to understand and control the seismic response of and define appropriate performance indices for inelastic and large-scale structures improved with TMDs. In that respect, this study evaluates the suitability of

four objective functions for the optimum design of the TMD of an inelastic, steel moment-resisting frame (SMRF) subjected to seismic loading. The objective functions include 1) the maximum roof lateral displacement, 2) the maximum drift, 3) the root mean square (RMS) of drifts and 4) the cumulative hysteretic energy of the SMRF. The TMD is first optimized under a white-noise excitation. The seismic response of the SMRF equipped with the optimized TMD is then further evaluated under four historic earthquake records.

2 Seismic energy approach

The earthquake input energy transmitted to a structure consists of four components: 1) kinetic energy, which reflects the work of the inertial force, 2) elastic strain energy, which is a recoverable potential energy stored in the structure in the form of elastic strain, 3) damping energy, which is the irreversible work of the damping force and 4) hysteretic (plastic) energy, which is the energy dissipated through inelastic excursions during the seismic excitation and is associated with the damage potential of the structure (Kuwamura and Galambos 1989). A TMD system can convert some of the earthquake input energy into damping energy and consequently reduce the structural damage caused by hysteretic energy. Therefore, the seismic design of structures with damping devices would best be based on an energy-based approach reflecting the distribution of input energy. In such approach, once the energy demand for a structure is estimated from the earthquake ground motion, the damage potential can be quantified by a combination of response and energy parameters. Sufficient strength and energy dissipation capacity should therefore be provided in the structure to achieve an acceptable damage threshold (i.e. a desired performance level – Khashaee et al. (2003)).

2.1 Seismic energy equation

The equation of motion of an n-DOF system is expressed as:

$$\mathbf{M}\ddot{\mathbf{u}}(t) + \mathbf{C}\,\dot{\mathbf{u}}\,(t) + \mathbf{F}_r(t) = -\mathbf{M}\mathbf{r}\ddot{x}_g(t) \tag{1}$$

where $\mathbf{M}$ is the non-zero, $n \times n$ mass matrix; $\mathbf{C}$ is the $n \times n$ viscous damping matrix; $\mathbf{F}_r(t)$ is the global nonlinear restoring force vector at time t; $\ddot{\mathbf{u}}(t), \dot{\mathbf{u}}(t)$ and $\mathbf{u}(t)$ are the response vectors of acceleration, velocity and displacement respectively; $\mathbf{r}$ is the support influence vector; and $\ddot{x}_g(t)$ is the ground acceleration at time t. Using the derivative relationships among displacement, velocity and acceleration:

$$d\mathbf{u}(t) = \dot{\mathbf{u}}\,(t)\,dt \tag{2}$$

$$d\,\dot{\mathbf{u}}\,(t) = \ddot{\mathbf{u}}(t)\,dt \tag{3}$$

Multiplying both sides of (1) by the transpose of displacement increment, $\dot{\mathbf{u}}^T(t)$, followed by integrating over the displacement domain from time 0 to time t_k, yields:

$$\int_0^{t_k} \dot{\mathbf{u}}^T(t)\,\mathbf{M}\ddot{\mathbf{u}}(t)dt + \int_0^{t_k} \dot{\mathbf{u}}^T(t)\,\mathbf{C}\,\dot{\mathbf{u}}\,(t)dt + \int_0^{t_k} \dot{\mathbf{u}}^T(t)\,\mathbf{F}_r(t)dt = -\int_0^{t_k} \dot{\mathbf{u}}^T(t)\,\mathbf{M}\mathbf{r}\ddot{x}_g(t)dt \tag{4}$$

The three terms of the left-hand side of (4) represent kinetic energy (E_k), damping energy (E_d) and absorbed energy (E_a), respectively, and the term on the right-hand side of (4) is considered as the input energy (E_i). Absorbed energy itself consists of elastic strain energy (E_s) and hysteretic energy (E_h). Therefore, the energy balance equation is rewritten as (Wong 2008):

$$E_k + E_d + E_a = E_i \tag{5}$$

where

$$E_k(t) = \int_0^{t_k} \dot{\mathbf{u}}^T(t)\,\mathbf{M}\ddot{\mathbf{u}}^T(t)dt \tag{6}$$

$$E_d(t) = \int_0^{t_k} \dot{\mathbf{u}}^T(t)\,\mathbf{C}\dot{\mathbf{u}}\,(t)dt \tag{7}$$

$$E_a(t) = \int_0^{t_k} \dot{\mathbf{u}}^T(t)\,\mathbf{F}_r(t)dt \tag{8}$$

$$E_i(t) = -\int_0^{t_k} \dot{\mathbf{u}}^T(t)\,\mathbf{M}\mathbf{r}\ddot{x}_g(t)dt \tag{9}$$

2.2 Computation of seismic hysteresis energy

A numerical approximation method proposed by Gong et al. (2013) was used to calculate the cumulative hysteresis energy of the structures examined in this study. This method uses the seismic response histories of the structural members to calculate their hysteretic energy dissipations that are later aggregated to calculate the cumulative (total) hysteretic energy of the entire structure. The hysteretic energy of the k-th element, $E_{h,k}$, of the structure is determined at the end of an earthquake using the total work of internal forces as:

$$E_{h,k} = W_{Moment,k} + W_{Axial,k} + W_{Shear,k} \;\; ; \;\; k = 1, 2, \ldots, n_e \tag{10}$$

where n_e is the number of elements; and $W_{Moment,\,k}$, $W_{Axial,\,k}$ and $W_{Shear,\,k}$ are the work done by the bending moment, axial force and shear force of the k-th element, respectively, and can be approximated as:

$$W_{Moment,k} = \sum_{t=0}^{T} \frac{1}{2}\left(\Delta\varphi_{t,k} + \Delta\varphi_{t-\Delta t,k}\right)M_{t,k} \tag{11}$$

$$W_{Axial,k} = \sum_{t=0}^{T} \frac{1}{2}\left(\Delta x_{t,k} + \Delta x_{t-\Delta t,k}\right) P_{t,k} \tag{12}$$

$$W_{Shear,k} = \sum_{t=0}^{T} \frac{1}{2}\left(\Delta y_{t,k} + \Delta y_{t-\Delta t,k}\right) V_{t,k} \tag{13}$$

where T is the duration of the earthquake; M_t, P_t and V_t are internal moment, axial force and shear force at time t, respectively; $\Delta\varphi$, Δx and Δy are the increments of end rotation, axial deformation, and shear deformation of the element from time $t-\Delta t$ to time t, respectively; and Δt is the time-increment for dynamic analysis. The cumulative hysteretic energy of the structure is then computed as:

$$E_h = \sum_{k=1}^{ne} E_{h,k} \tag{14}$$

3 Optimal design of a TMD system

3.1 Optimization problem

Four different performance indices were used and compared against as the objective function of an optimization problem seeking the optimum values for the parameters of a TMD system of a six-story, inelastic SMRF subjected to an earthquake excitation. The objective functions included 1) minimizing the maximum roof lateral displacement (denoted here as RoofDisp), 2) minimizing the maximum drift (denoted here as Drift), 3) minimizing the root mean square of drifts (denoted here as RMSDrifts) and 4) minimizing the cumulative hysteretic energy of the SMRF (denoted here as TotHysE). The minimization problem for the four cases can then be expressed as:

$$\begin{aligned}
&\text{Find}: \quad m_d, k_d, c_d \\
&\text{Minimize}: \\
&\quad \text{RoofDisp}: \quad f(m_d,k_d,c_d) = \max\left(\left|x_{roof}(t)\right|\right);\ \ t = 0, \Delta t, 2\Delta t, \ldots, T \\
&\quad \text{Drift}: \quad f(m_d,k_d,c_d) = \max\left(\left|D_i(t)\right|\right)\ ;\ \ t = 0, \Delta t, 2\Delta t, \ldots, T; i = 1, 2, \ldots, N_{\text{story}} \\
&\quad \text{RMSDrifts}: \quad f(m_d,k_d,c_d) = \max\left(\sqrt{\frac{\sum_{t=0}^{T} D_i(t)^2}{T}}\right);\ \ t = 0, \Delta t, 2\Delta t, \ldots, T; i = 1, 2, \ldots, N_{\text{story}} \\
&\quad \text{TotHysE}: \quad f(m_d,k_d,c_d) = E_h \\
&\text{subject to}: \\
&\quad x_{\max,\text{TMD}}(m_d,k_d,c_d) \le x_{all} \\
&\quad m_{d,\min} \le m_d \le m_{d,\max} \\
&\quad 0 < k_d \le k_{d,\max} \\
&\quad 0 < c_d \le c_{d,\max}
\end{aligned} \tag{15}$$

where $m_{d,\ \min}$ and $m_{d,\ \max}$ are the lower and upper bounds of the TMD mass, m_d; $k_{d,\ \max}$ is the upper bound of the TMD stiffness, k_d; $C_{d,\max}$ is the upper bound of the TMD damping, c_d; $x_{\max,\ \text{TMD}}$ and x_{all} are the maximum and allowable values of stroke length for TMD; $x_{roof}(t)$ is the lateral displacement of the top story (roof) in time t; $D_i(t)$ is the drift of the i-th story in time t; and N_{story} is the number of stories of the structure.

3.2 Constraint-handling approach

Numerous constraint-handling techniques have been proposed in the literature for metaheuristic algorithms. Examples include dynamic penalties and adaptive penalties. The interested reader is referred to a comprehensive survey by Coello Coello (2002). In this study, one of the most efficient forms of penalty functions used structural optimization known the external penalty function was used (Yazdani et al. 2017; Khatibinia and Yazdani 2018). This penalty function converts the constrained optimization problem of the TMD system into an unconstrained one as:

$$\tilde{f}(m_d,k_d,c_d) = f(m_d,k_d,c_d)\left(1 + r_p P_f\right) \tag{16}$$

where $\tilde{f}$ is the penalized objective function of a constraint-violating solution, and r_p is an adjusting coefficient defined as (Chen and Chen 1997):

$$r_p = r_{p1}\left[1 + 0.2(l-1)\right] \le 4 r_{p1} \tag{17}$$

where r_{p1} is an initial adjusting value in the first iteration, and l is the generation counter. In (16), P_f is the total penalty and represents the degree of constrain violation and defined as:

$$P_f = \frac{x_{\max,TMD}}{x_{all}} - 1 \tag{18}$$

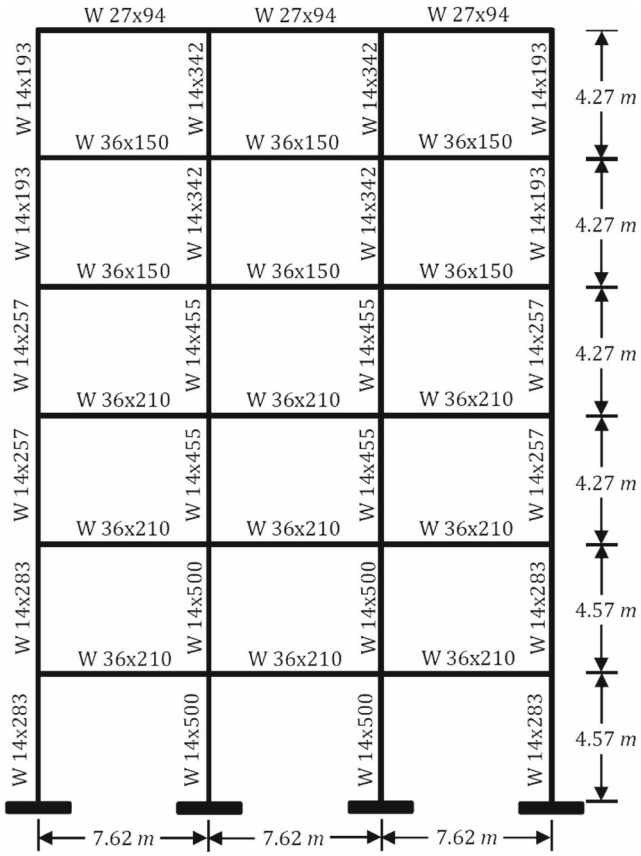

Fig. 1 Six-story SMRF model

4 Particle swarm optimization algorithm

The particle swarm optimization (PSO) has widely been used as an efficient technique in structural optimization (e.g. Gharehbaghi and Khatibinia (2015); Mokarram and Banan (2018)). Introduced by Kennedy and Eberhart (1995), PSO

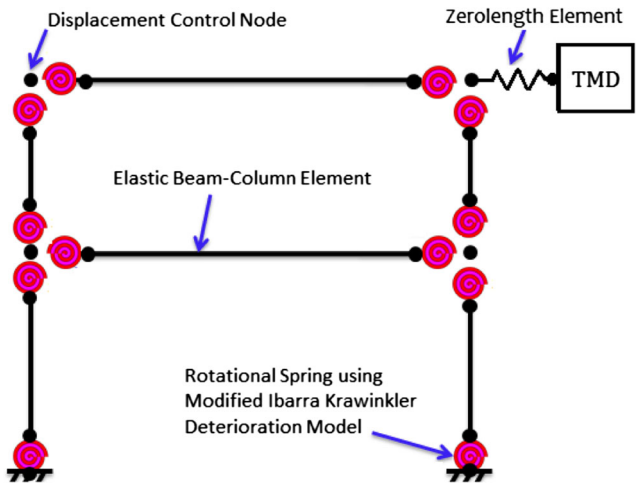

Fig. 2 TMD-equipped SMRF model with lumped plasticity

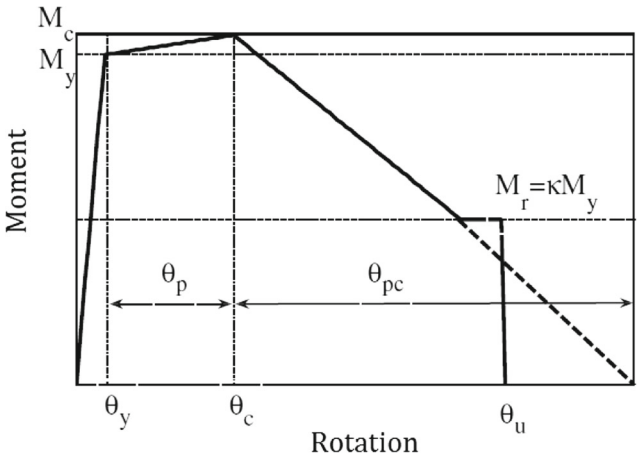

Fig. 3 Monotonic moment-rotation relationship for the modified IMK deterioration model (Ibarra et al. 2005; Lignos and Krawinkler 2011)

imitates the choreography and sociocognitive behavior of birds in a flock. The birds in the flock are called particles and represent possible solutions in the search space. Particles quasi-randomly fly around and iteratively move toward the optimum solution (food). They keep an eye on others to follow the particle closest to the optimum solution (g_{best}) while keeping track of their own best solutions found so far (p_{best}). The i-th particle in the l-th iteration is associated with a position vector, $\boldsymbol{X}_i^l$, and a velocity vector, $\boldsymbol{V}_i^l$, denoted as:

$$\begin{aligned} \boldsymbol{X}_i^l &= \left\{ x_{i,1}^l, x_{i,2}^l, \ldots, x_{i,p}^l \right\} \\ \boldsymbol{V}_i^l &= \left\{ v_{i,1}^l, v_{i,2}^l, \ldots, v_{i,p}^l \right\} \end{aligned} \tag{19}$$

where p is the dimension of the solution space. As the particle flies through the solution space, its position is updated as:

$$\boldsymbol{V}_i^{l+1} = \omega^l \boldsymbol{V}_i^l + c_1 r_1 \left(\boldsymbol{pbest}_i^l - \boldsymbol{X}_i^l \right) + c_2 r_2 \left(\boldsymbol{gbest}^l - \boldsymbol{X}_i^l \right) \tag{20}$$

$$\boldsymbol{X}_i^{l+1} = \boldsymbol{X}_i^l + \boldsymbol{V}_i^{l+1} \tag{21}$$

where r_1 and r_2 are two uniform random numbers between (0, 1); c_1 and c_2 are the cognitive- and social-scaling parameters,

Table 1 The benchmark SMRF's natural periods of vibration

Mode number	Natural periods of vibration (s)	
	Wong (2008)	Present study
1	1.22	1.24
2	0.44	0.45
3	0.25	0.25
4	0.18	0.18
5	0.14	0.14
6	0.11	0.11

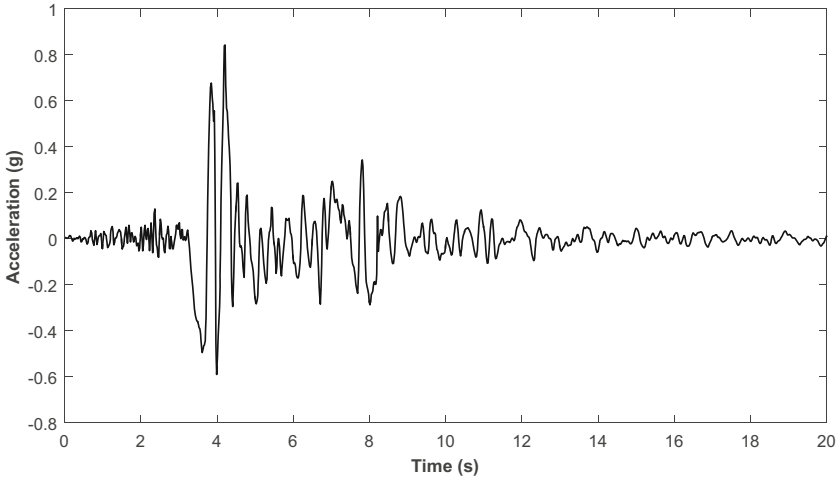

Fig. 4 The 1994 Northridge ground motion record as used by Wong (2008)

respectively; and ω^l is the inertia weight that controls the influence of the previous velocity and is defined in the l-th iteration as (Shi and Eberhart 1998):

$$\omega = \omega_{\max} - \frac{\omega_{\max} - \omega_{\min}}{l_{\max}}\, l \tag{22}$$

where $\omega_{\max}$ and $\omega_{\min}$ are the maximum and minimum values of ω, respectively; and l_{max} is the maximum number of iterations.

A passive-congregation-based PSO (PSOPC) proposed by He et al. (2004) was used in the present study. The passive congregation is an important biological force that preserves a flock's integrity by attracting particles to the flock. Compared with PSO, PSOPC exhibits an improved accuracy and a faster convergence rate. In PSOPC, the velocity is modified as:

$$\boldsymbol{V}_i^{l+1} = \omega^l \boldsymbol{V}_i^l + c_1 r_1 \left(\boldsymbol{pbest}_i^l - \boldsymbol{X}_i^l\right) + c_2 r_2 \left(\boldsymbol{gbest}^l - \boldsymbol{X}_i^l\right) + c_3 r_3 \left(\boldsymbol{R}_i^l - \boldsymbol{X}_i^l\right) \tag{23}$$

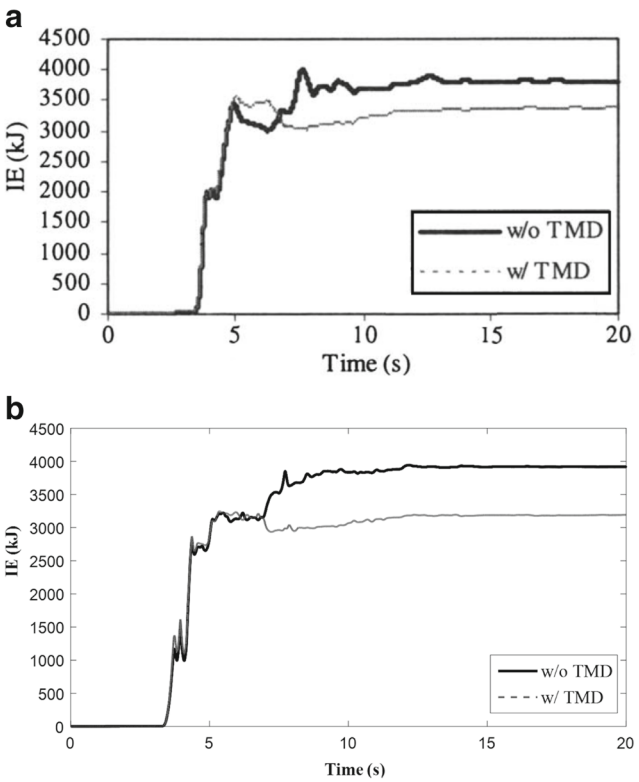

Fig. 5 Time history of input energy for the Northridge earthquake: **a** Wong (2008), with permission from ASCE and **b** this study

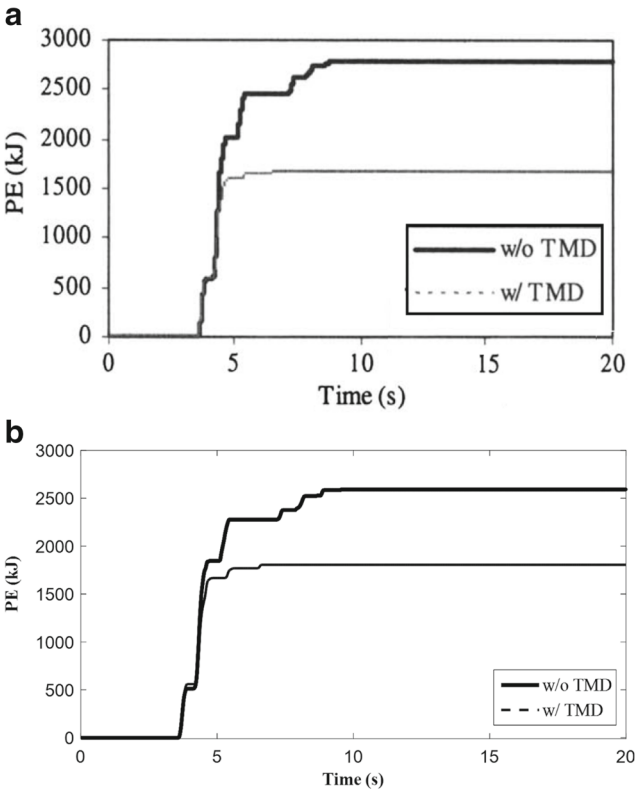

Fig. 6 Time history of cumulative hysteresis energy for the Northridge earthquake: **a** Wong (2008), with permission from ASCE and **b** this study

Table 2 Lower and upper bounds of the values of TMD parameters

TMD Parameter	Lower bound	Upper bound
c_d (MN.s/m)	0	2
k_d (MN/m)	0	40
m_d (ton)	9	180

where $\boldsymbol{R}_i$ is a particle selected randomly from the swarm; c_3 is the passive congregation coefficient; and r_3 is a uniform random number in the range (0, 1).

5 Modeling a benchmark SMRF equipped with TMD

The TMD-equipped, six-story SMRF used by Wong (2008) was employed as a benchmark in this study (Fig. 1).

The open-source finite element software OpenSEES (Mazzoni et al. 2006) was used for the nonlinear dynamic analysis of the SMRF. Plasticity was introduced in the structural elements using a lumped plasticity model, which assumes zero-length plastic hinges (rotational springs) at the ends of elastic beam-column elements (Fig. 2).

The hinges obeyed a bilinear hysteretic behavior based on the Ibarra–Medina–Krawinkler (IMK) model (Ibarra et al. 2005). The properties of the IMK model are shown in Fig. 3. The model considers nonlinearity by five marked parameters including 1) the pre-capping (i.e. pre-maximum moment) plastic rotation (θ_p), 2) the post-capping (i.e. from maximum moment to fracture) plastic rotation (θ_{pc}), 3) the cumulative rotation capacity (κ), which determines the reference energy dissipation capacity of a structural element, 4) the ratio of the effective (actual) to estimated yield stress ($M_y/M_{y,\ p}$) and 5) the post-yield (maximum) strength ratio (M_c/M_y).

Table 3 Optimum parameters of the TMD system for the four objective functions

Objective function	Optimum value of the TMD parameter		
	m_d (ton)	k_d (MN/m)	c_d (MN.s/m)
RoofDisp	180	3.55	0.24
Drift	180	3.42	0.25
RMSDrifts	180	2.55	0.26
TotHysE	180	1.95	0.45
Mean	180	2.87	0.30

A mass of 300 t was assumed for each story, and the damping of the structure was assumed to be 3%. A yield stress of 248.2 MPa and an elasticity modulus of 2×10^5 MPa were considered for steel, and a uniformly-distributed load of 21.89 kN/m was applied on the beams. The TMD system was modeled using a node defined at the roof level with a concentrated mass assigned to it and connected to its corresponding structural node using a zero-length element (Fig. 2). The rotation and displacement of the node were assumed to be equal to those of the corresponding structural node, while the stiffness of the TMD system was assigned to the zero-length element. The damping of the TMD system was defined using a viscous material. The damping matrix of the TMD-equipped SMRF was then obtained using the Rayleigh method (Clough and Penzien 1975).

Two numerical measures were used to validate the SMRF model. First, the natural periods of vibration corresponding to its first six modes of the elastic structure were computed and juxtaposed with those reported by Wong (2008). The results summarized in Table 1 indicate the close agreement between the two series of natural periods of vibration.

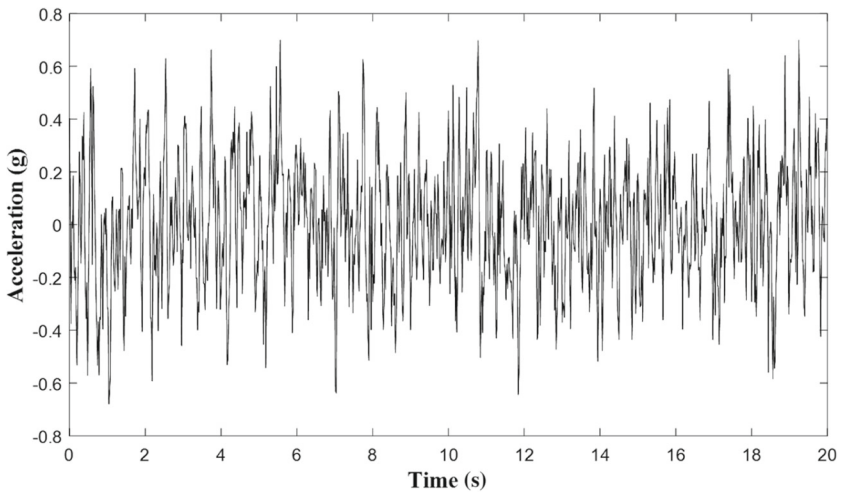

Fig. 7 Time history of white-noise ground acceleration with a peak ground acceleration of 0.7 *g*

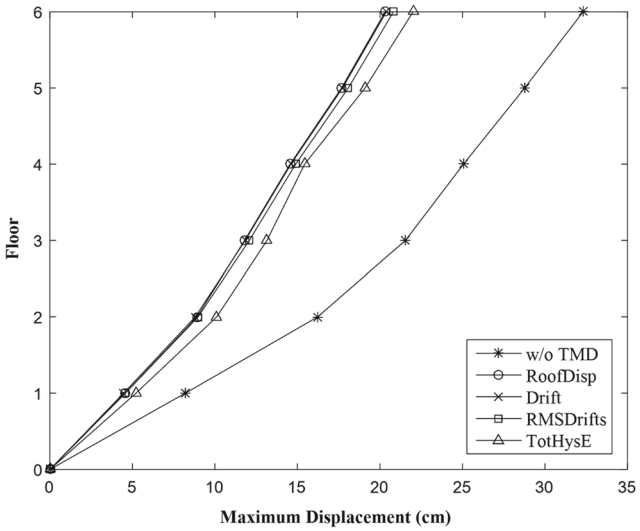

Fig. 8 Maximum lateral displacement of stories under the artificial earthquake

In addition, a time-history analysis was carried out under the 1994 Northridge earthquake record (Fig. 4) used by Wong (2008) to compare the time history of the input and cumulative hysteresis energies of the model with and without a TMD with those obtained by Wong (2008).

The results shown in Figs. 5 and 6 indicate similar trends and variations in the seismic input energy during the earthquake ground motion. Figure 6 also shows that the cumulative hysteresis energy obtained based on the numerical approximation given in (10) to (13) matches that of Wong (2008). The results of the validation experiments were deemed adequate to confirm the accuracy of the SMRF model created and used in this study.

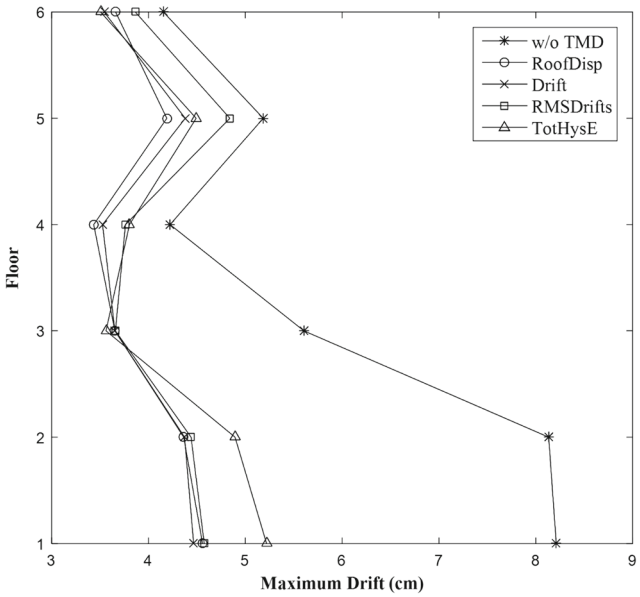

Fig. 9 Maximum drift of stories under the artificial earthquake

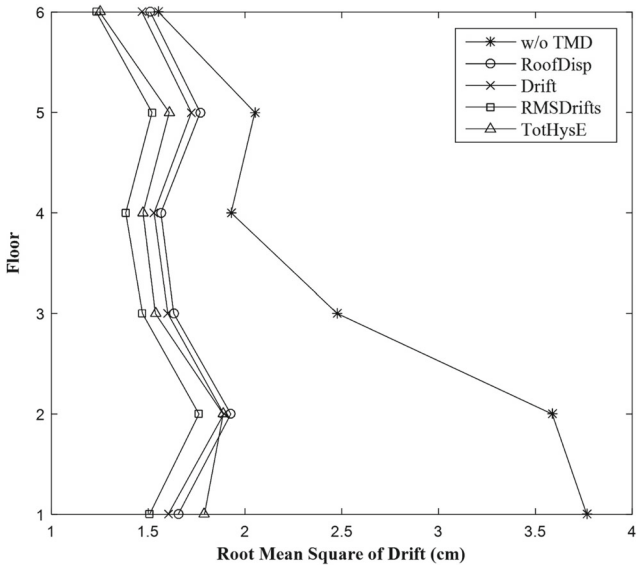

Fig. 10 Maximum RMS of story drifts under the artificial earthquake

6 Optimization results

6.1 Optimum design of TMD under an artificial earthquake

The upper and lower bounds for the mass, stiffness and damping of the subject TMD are shown in Table 2. The lower and upper bounds of the TMD's mass corresponded with 0.5 and 10% (based on Wong (2008)) of the structure's total mass, respectively. As reported by Mohebbi and Joghataie (2012), TMD's mass has a considerable influence on the TMD's optimum design where larger stiffness and damping values are associated with heavier TMDs. In the present study, relatively large values were used for the upper bound of the TMD's stiffness and damping to accommodate room for uncertainty and paucity of knowledge about the potential influences of the structure's inelastic behavior on the TMD's optimum design.

A maximum allowable displacement of $x_{all} = 175$ cm relative to the roof displacement was applied for the TMD. In the PSOPC algorithm, the population size (N) and the maximum number of iterations (l_{max}) were set to 30 and 150, respectively. The upper and lower bounds for the inertia weight (i.e. $\omega_{\max}$ and $\omega_{\min}$) and r_{p1} were set to 0.4, 0.1 and 25, respectively. These parameters were selected based on general recommendations given in the literature (e.g. Gharehbaghi and Khatibinia (2015)).

The optimum values for the TMD parameters are evidently specific to the earthquake record used. In this study, first the TMD parameters were optimized under an artificial stationary earthquake excitation, $\ddot{x}_g(t)$, and then the nonlinear response of the SMRF equipped with the optimized TMD was evaluated under a few historic earthquake records.

The artificial stationary earthquake excitation was modeled as a white-noise signal with constant spectral density, S_0,

Table 4 Maximum absolute displacements for different objective functions and their corresponding improvement percentages relative to the uncontrolled SMRF

Story	Maximum absolute displacement (cm)					Reduction (%)			
	No TMD	With TMD				With TMD			
		RoofDisp	Drift	RMSDrifts	TotHysE	RoofDisp	Drift	RMSDrifts	TotHysE
1	8.2	4.5	4.4	4.5	5.2	44.4	45.6	44.2	36.4
2	16.2	8.9	8.8	8.9	10.1	45.0	45.7	44.6	37.7
3	21.5	11.8	11.8	12.0	13.1	45.2	45.0	43.9	38.9
4	25.1	14.5	14.6	14.8	15.4	41.9	41.7	40.5	38.4
5	28.7	17.6	17.7	18.0	19.0	38.5	38.3	37.1	33.6
6	32.3	20.3	20.3	20.8	22.0	37.1	36.8	35.5	31.8
					Mean	42.1	42.2	41.0	36.2

filtered through the Kanai-Tajimi model (Tajimi 1960; Kanai 1961). The power spectral density (PSD) function was determined using the following equation:

$$S_{K.T}(\omega) = S_0 \left[\frac{{\omega_g}^4 + 4{\zeta_g}^2{\omega_g}^2\omega^2}{\left(\omega^2 - {\omega_g}^2\right)^2 + 4{\zeta_g}^2{\omega_g}^2\omega^2} \right] \; ; \quad S_0 = \frac{0.03\zeta_g}{\pi\omega_g\left(4{\zeta_g}^2 + 1\right)} \tag{27}$$

where ζ_g and ω_g are the ground damping and frequency, respectively. The values of 0.8 and 25.13 rad/s (4 Hz) were used for these parameters, respectively. These values were selected based on the recommendations of Wu et al. (1999) assuming the site class C (very dense soil and soft rock - ASCE 7-16 (2016)) for the location of the frame. The artificial earthquake was not matched to a design spectrum. The generated earthquake record had a peak ground acceleration, PGA, of 0.7 g (Fig. 7). The artificial earthquake was subsequently applied on the TMD-equipped SMRF.

Given the stochastic nature of the PSOPC algorithm, 10 independent runs were conducted for each objective function (i.e. 40 runs in total) and the values for the parameters of the TMD system were computed. The parameters corresponding to the minimum objective function were then selected as the global optimum parameters of the TMD system. The optimum values obtained for each objective function are given in Table 3.

The results indicate that the optimum mass for the TMD in all cases is equal to the upper bound selected for this parameter. This observation is due to the commensurateness of the mass of a TMD with how effectively it would mitigate structural responses (Mohebbi and Joghataie 2012). However, the TMD mass should usually be limited to avoid increasing the total weight of the structure that can in turn cause TMD-structure dynamic interactions.

Figures 8, 9 and 10 show the variations of the maximum roof lateral displacement, the maximum drift and the RMS of drifts along the height of the SMRF under the artificial earthquake and for different objective functions.

Table 5 Maximum absolute drifts for different objective functions and their corresponding improvement percentages relative to the uncontrolled SMRF

Story	Maximum absolute drift (cm)					Reduction (%)			
	Without TMD	With TMD				With TMD			
		RoofDisp	Drift	RMSDrifts	TotHysE	RoofDisp	Drift	RMSDrifts	TotHysE
1	8.2	4.5	4.4	4.5	5.2	44.5	45.6	44.2	36.4
2	8.1	4.3	4.3	4.4	4.8	46.3	46.2	45.4	39.8
3	5.6	3.6	3.6	3.6	3.5	34.8	34.8	34.7	36.4
4	4.2	3.4	3.5	3.7	3.8	18.6	16.5	10.9	9.9
5	5.1	4.1	4.3	4.8	4.4	19.2	15.5	6.6	13.3
6	4.1	3.6	3.5	3.8	3.5	11.8	14.7	6.9	15.6
					Mean	29.2	28.9	24.8	25.2

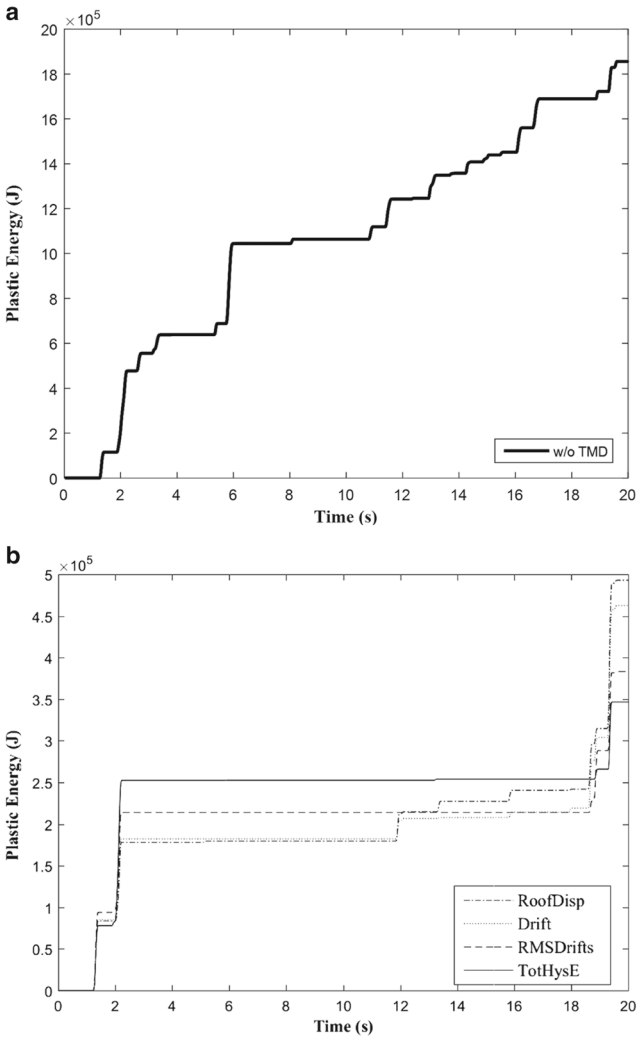

Fig. 11 The time history of the cumulative hysteresis under the artificial earthquake for **a** the uncontrolled and **b** the TMD-equipped structures

To help the reader better discern the data, the results shown in Figs. 8 and 9 together with additional statistical analyses are also presented in Tables 4 and 5. The results indicate that the optimized TMD considerably mitigated the maximum responses of the frame under the artificial earthquake. Mean reductions of 36 to 42% and 25 to 29% were achieved for the maximum roof displacements (Table 4) and the maximum drifts (Table 5), respectively. In addition, the results in Fig. 8 and Table 4, which correspond to the maximum roof displacements, indicate that the story displacements of the SMRF equipped with a TMD increased linearly with height. Put other way, comparable drifts were observed for all floors of the TMD-equipped SMRF, as shown in Figs. 9 and 10 and Table 5. In contrast, the first three stories of the uncontrolled SMRF experienced considerably larger drifts compared with the upper three floors, resulting in a nonlinear deformed shape for the structure.

Table 7 Comparison of mean improvement values obtained by objective functions

Performance index	Objective functions			
	RoofDisp	Drift	RMSDrifts	TotHysE
Maximum absolute displacement	42.1	42.2	41.0	36.2
Maximum absolute drift	29.2	28.9	24.8	25.2
Cumulative hysteresis energy	73.5	75.1	79.4	81.3
Mean	48.3	48.7	48.4	47.6

Figure 11 and Table 6 show the hysteresis energy accumulated in the SMRF during the artificial earthquake for each objective function. The results provide another evidence for the considerable efficacy of the optimized TMD in mitigating the seismic structural responses of the frame and protecting it from major damages. Quantitatively, the TMD optimized based on the cumulative hysteresis energy as the objective function reduced the cumulative plastic energy dissipation by 81.3% from 1855.9 kJ in the uncontrolled SMRF to 346.6 kJ. This reduction is considerably greater than the mean reductions obtained for other performance indices. The other objective functions produced comparable reductions for energy dissipation.

The mean values produced by the objective functions for each performance index (except RMS of drifts) are summarized in Table 7 where their grand means are also shown as a figure of merit for the objective functions. The results indicate that all the objective functions exhibited roughly the same performances in mitigating seismic structural responses.

Similar to the performance indices, the maximum story accelerations of the SMRF were also observed to be considerably reduced by equipping the structure with the optimized TMD (Fig. 12). Similar trends can be seen in the variations of the maximum story accelerations along the height of the SMRF: the roof and the first floor experienced the largest and smallest accelerations, respectively, while the other stories underwent roughly the same accelerations. Except the roof,

Table 6 Cumulative hysteresis energies for different objective functions and their corresponding improvement percentages with respect to the uncontrolled SMRF

Cumulative hysteresis energy (kJ)					Reduction (%)			
Without TMD	With TMD				With TMD			
	RoofDisp	Drift	RMSDrifts	TotHysE	RoofDisp	Drift	RMSDrifts	TotHysE
1855.9	492.8	462.5	383.2	346.6	73.5	75.1	79.4	81.3

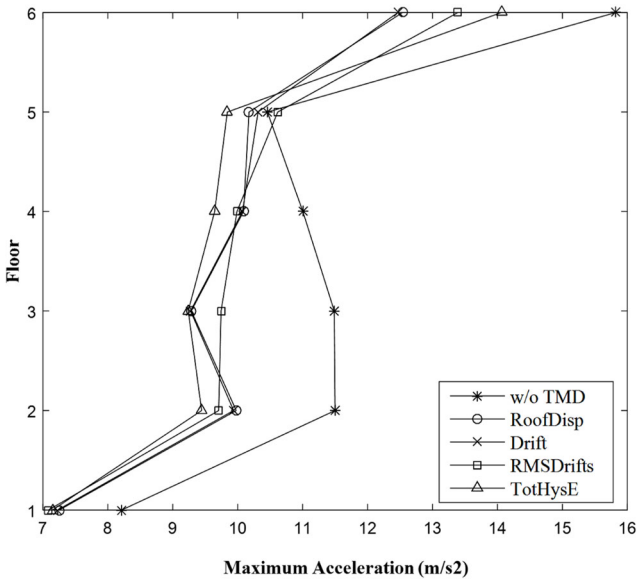

Fig. 12 Maximum acceleration of stories under the artificial earthquake

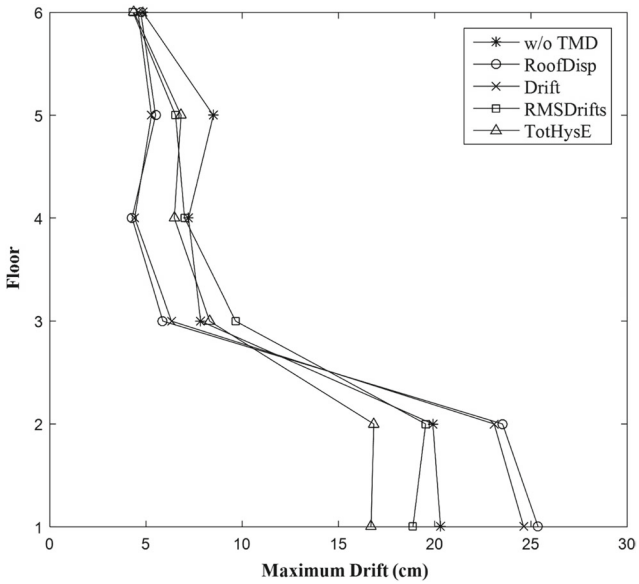

Fig. 13 Maximum drift of stories under the Kobe earthquake

cumulative hysteresis energy resulted in the lowest accelerations across the frame.

Considering the results shown and summarized in Figs. 8, 9, 10, 11 and 12 and Table 7, all the objective functions seem effective in mitigating seismic structural responses. However, because even small reductions in the plastic energy of a structure could translate into sizably lower damages, cumulative hysteresis energy, which resulted in the minimum plastic energy, was deemed the most effective objective function under an artificial excitation.

6.2 Assessment of SMRF equipped with optimized TMD under real earthquake excitations

The assessment of the TMD-equipped SMRF was further examined under four historic earthquake records: two near-field earthquakes of Kobe and Niigata and two far-filed earthquakes of Tabas and Northridge (Table 8). The earthquake records were selected had the same site class (i.e. C) as assumed for the artificial earthquake. It should be noted that the Northridge earthquake record given in Table 8 is different from that used by Wong (2008), which was employed earlier to validate the model.

Figs. 13, 14, 15 and 16 show the maximum drifts of the SMRF in both uncontrolled and TMD-equipped forms under the real earthquakes. The results show that the near-field Kobe earthquake caused the largest drifts in the uncontrolled structure. This observation could be attributed to the distinct, short-duration, long-period, large-amplitude pulses that near-field ground motions contain in both velocity and displacement. The results also indicate that equipping a structure with a TMD optimized using an artificial earthquake will not warrant that the structure will exhibit a better seismic performance in any measure compared with when no TMD is used. For instance, Figs. 13 and 15 indicate that the SMRF equipped with a TMD optimized using the objective functions RoofDisp and Drift exhibited larger drifts for the first two floors under the Kobe and Northridge earthquakes compared with the non-equipped SMRF. A similar observation is made from Figs. 14 and 15 for the fifth floor when the structure is subjected to the Niigata and Tabas earthquakes. A closer look at the results suggests that the results of the objective functions

Table 8 Properties of the real earthquakes

Earthquake	Year	Station	T_p (s)	Duration (s) 5–95%	PGA[a] (g)	M_w	R_{rup} (km)	V_{s30} (m/s)	Scale factor
Kobe, Japan	1995	Takatori	1.554	11.3	0.67	6.9	1.47	256	1
Niigata, Japan	2004	NIG019	–	96.8	1.33	6.63	9.88	372.33	1
Northridge, USA	1994	Los Angeles	–	11.6	1.87	6.69	27.01	308.71	4
Tabas, Iran	1978	Boshrooyeh	–	19.5	0.53	7.35	28.79	324.57	5

[a] larger horizontal component

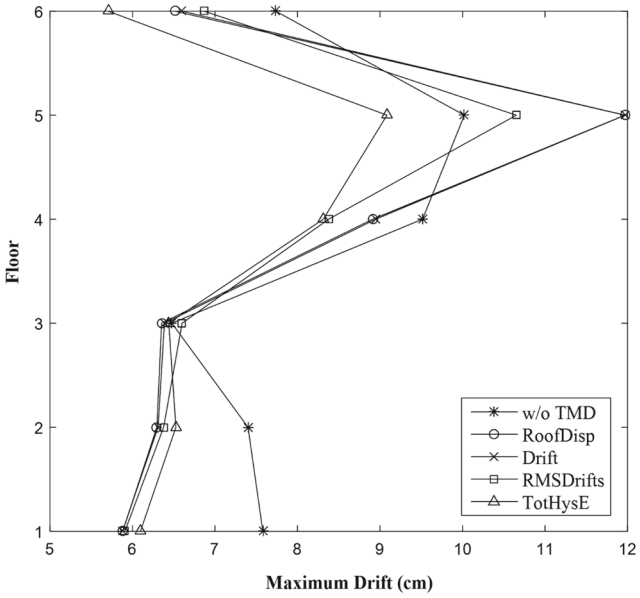

Fig. 14 Maximum drift of stories under the Niigata earthquake

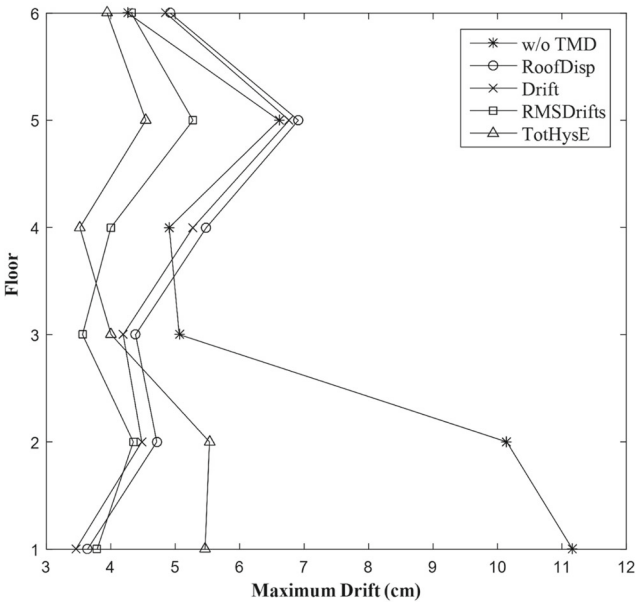

Fig. 16 Maximum drift of stories under the Tabas earthquake

RoofDisp and Drift form one cluster, while the other two objective functions (i.e. RMSDrifts and TotHysE) form another, implying an interconnectedness within each cluster. It can also be seen that, under all the real earthquakes, TotHysE was the only objective function that yielded a TMD that consistently reduced drifts to smaller levels than them of the uncontrolled structure. The other objective functions did not yield a TMD with such consistency.

The cumulative hysteresis (plastic) energies of the SMRF with and without a TMD under the historic earthquakes are shown in Figs. 17, 18, 19 and 20. Granting that plastic energy is associated with the damage experienced by a structure (Kuwamura and Galambos 1989), the results show that the non-equipped TMD underwent the most damage under the Kobe earthquake followed by the Niigata, Northridge and Tabas earthquakes. The results also corroborate the efficacy of a TMD in reducing cumulative hysteresis energy and in turn mitigating potential damages to the structure under real earthquakes. Similar clusters of curves as those seen in Figs. 13, 14, 15 and 16 are observed in Figs. 17, 18, 19 and 20 where the objective functions RoofDisp and Drift produce

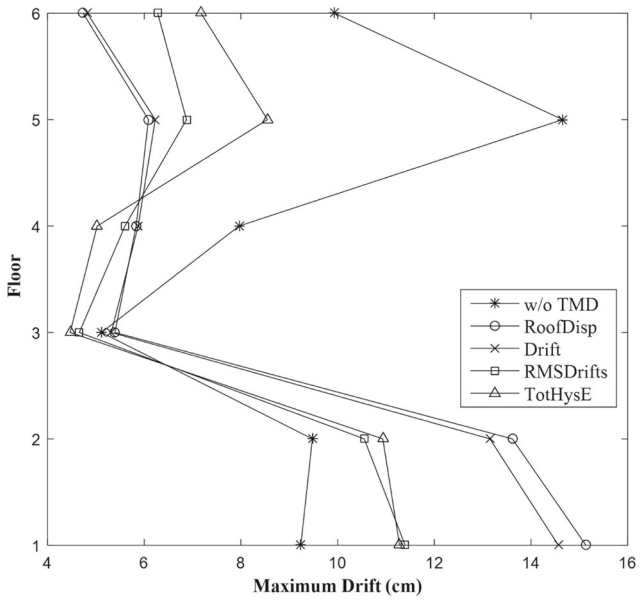

Fig. 15 Maximum drift of stories under the Northridge earthquake

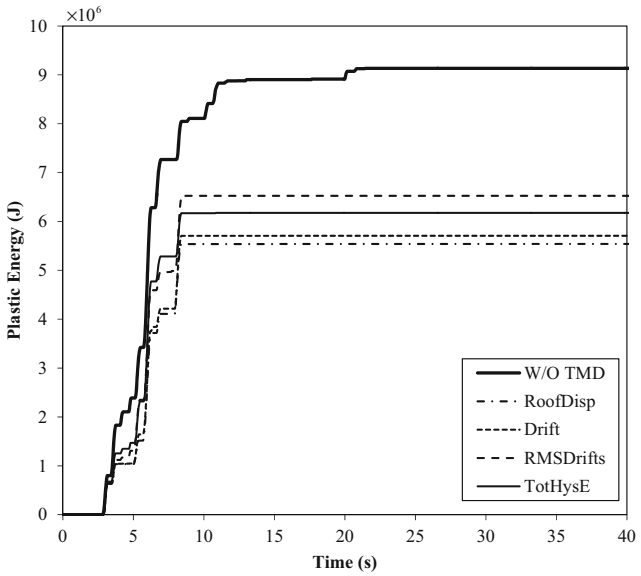

Fig. 17 Time history of cumulative hysteresis energy under the Kobe earthquake

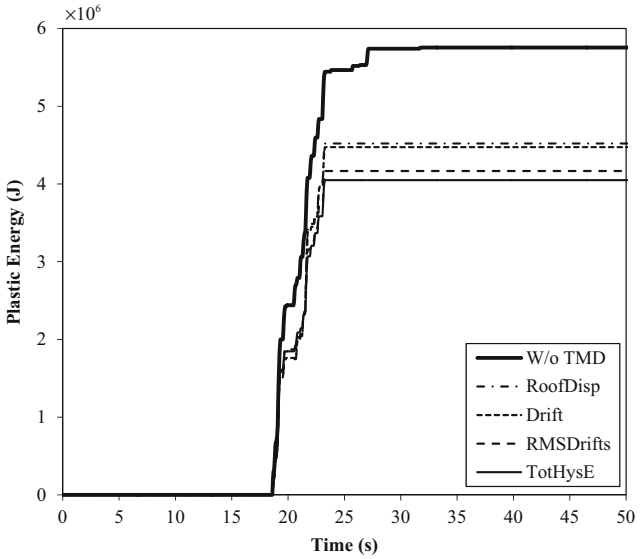

Fig. 18 Time history of cumulative hysteresis energy under the Niigata earthquake

similar results different from those produced by the other two objective functions (i.e. RMSDrifts and TotHysE). A comparison of the results shows that none of the objective functions consistently resulted in the lowest cumulative hysteresis energy for all earthquakes. This observation indicates that the efficacy of a TMD depends on the characteristics of the earthquake excitation where the energy dissipation capacity of a TMD is inversely proportional to the strength of an earthquake shaking. Observing similar results, Wong and Harris (2010) attributed this behavior to detuning effects that occur during strong earthquakes due to major structural damages and, in turn, significant period shifts.

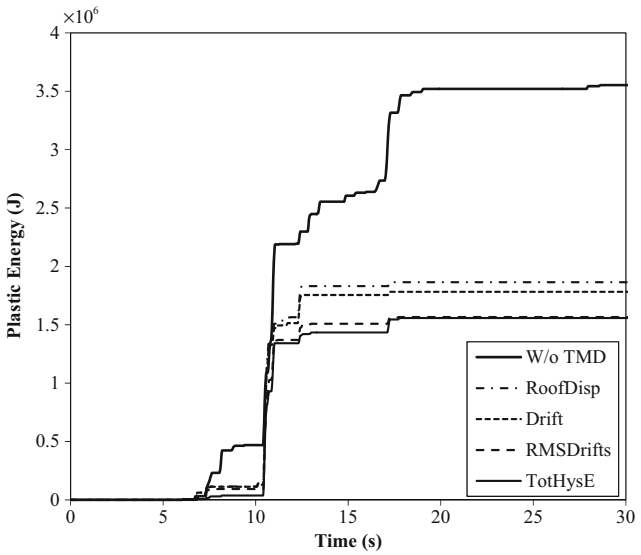

Fig. 19 Time history of cumulative hysteresis energy under the Northridge earthquake

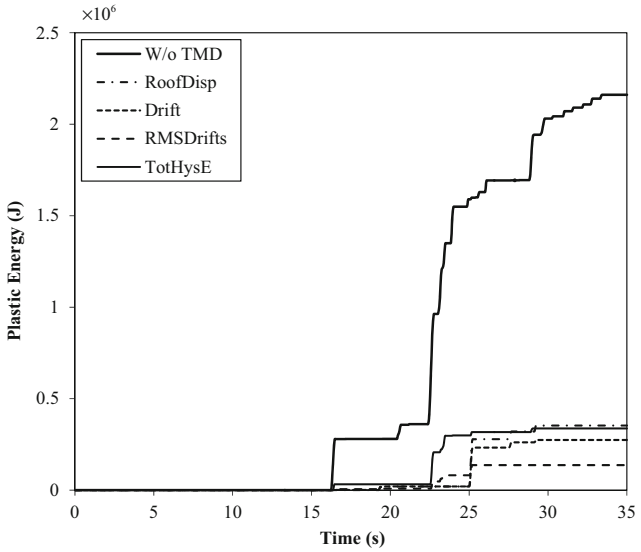

Fig. 20 Time history of cumulative hysteresis energy under the Tabas earthquake

7 Conclusions

A tuned mass damper was optimized for use in an inelastic steel moment-resisting frame (SMRF) subjected to a white-noise excitation using four different objective functions: 1) minimizing the maximum roof lateral displacement, 2) minimizing the maximum drift, 3) minimizing the root mean square of drifts and 4) minimizing the cumulative hysteretic energy of the SMRF. The seismic response of the SMRF equipped with the optimized TMD was further investigated under four historic earthquake records. The results indicated that the optimized TMD considerably mitigated the seismic response of the frame under the artificial earthquake. Mean reductions of 36 to 42% and 25 to 29% were achieved for the maximum roof displacements and the maximum drifts, respectively. The TMD optimized based on the cumulative hysteresis energy as the objective function reduced the cumulative plastic energy dissipation by 81.3%. The maximum story accelerations of the SMRF were also observed to be considerably reduced by equipping the structure with the optimized TMD. Assessment of the response of the TMD-equipped SMRF to the four historic earthquake records indicated that equipping a structure with a TMD optimized using an artificial earthquake will not guarantee that the structure will exhibit a better seismic performance in any measure compared with when no TMD is used. It was observed that the efficacy of a TMD depends on the characteristics of the earthquake excitation where the energy dissipation capacity of a TMD decreases as the earthquake shaking becomes stronger. This behavior was attributed to detuning effects arising from major structural damages and significant period shifts that in turn occur during strong earthquakes.

References

Aldwaik M, Adeli H (2014) Advances in optimization of highrise building structures. Struct Multidiscip Optim 50:899–919. https://doi.org/10.1007/s00158-014-1148-1

ASCE 7-16 (2016) Minimum design loads and associated criteria for buildings and other structures, 7th edn. American Society of Civil Engineers, Reston

Bakre SV, Jangid RS (2007) Optimum parameters of tuned mass damper for damped main system. Struct Control Health Monit 14:448–470. https://doi.org/10.1002/stc.166

Bekdaş G, Nigdeli SM (2011) Estimating optimum parameters of tuned mass dampers using harmony search. Eng Struct 33:2716–2723. https://doi.org/10.1016/j.engstruct.2011.05.024

Bekdaş G, Nigdeli SM (2017) Metaheuristic based optimization of tuned mass dampers under earthquake excitation by considering soil-structure interaction. Soil Dyn Earthq Eng 92:443–461. https://doi.org/10.1016/j.soildyn.2016.10.019

Bekdaş G, Nigdeli SM, Yang X-S (2018) A novel bat algorithm based optimum tuning of mass dampers for improving the seismic safety of structures. Eng Struct 159:89–98. https://doi.org/10.1016/j.engstruct.2017.12.037

Chen T-Y, Chen C-J (1997) Improvements of simple genetic algorithm in structural design. Int J Numer Methods Eng 40:1323–1334. https://doi.org/10.1002/(SICI)1097-0207(19970415)40:7<1323::AID-NME117>3.0.CO;2-T

Clough RW, Penzien J (1975) Dynamics of structures. McGraw-Hill Companies, New York

Coello Coello CA (2002) Theoretical and numerical constraint-handling techniques used with evolutionary algorithms: a survey of the state of the art. Comput Methods Appl Mech Eng 191:1245–1287. https://doi.org/10.1016/S0045-7825(01)00323-1

Den Hartog JP (1956) Mechanical vibrations, 4th edn. McGraw-Hill, New York

Desu NB, Deb SK, Dutta A (2006) Coupled tuned mass dampers for control of coupled vibrations in asymmetric buildings. Struct Control Health Monit 13:897–916. https://doi.org/10.1002/stc.64

Farshidianfar A, Soheili S (2013) Ant colony optimization of tuned mass dampers for earthquake oscillations of high-rise structures including soil–structure interaction. Soil Dyn Earthq Eng 51:14–22. https://doi.org/10.1016/j.soildyn.2013.04.002

Gharehbaghi S, Khatibinia M (2015) Optimal seismic design of reinforced concrete structures under time-history earthquake loads using an intelligent hybrid algorithm. Earthq Eng Eng Vib 14:97–109. https://doi.org/10.1007/s11803-015-0009-2

Gong Y, Xue Y, Xu L (2013) Optimal capacity design of eccentrically braced steel frameworks using nonlinear response history analysis. Eng Struct 48:28–36. https://doi.org/10.1016/j.engstruct.2012.10.001

Gupta Y, Chandrasekaren A (1969) Absorber system for earthquake excitation. In: The fourth world conference on earthquake engineering. Santiago, Chile, pp 139–148

He S, Wu QH, Wen JY et al (2004) A particle swarm optimizer with passive congregation. Biosystems 78:135–147. https://doi.org/10.1016/j.biosystems.2004.08.003

Ibarra LF, Medina RA, Krawinkler H (2005) Hysteretic models that incorporate strength and stiffness deterioration. Earthq Eng Struct Dyn 34:1489–1511. https://doi.org/10.1002/eqe.495

Kamgar R, Samea P, Khatibinia M (2017) Optimizing parameters of tuned mass damper subjected to critical earthquake. Struct Design Tall Spec Build. https://doi.org/10.1002/tal.1460

Kanai K (1961) An empirical formula for the spectrum of strong earthquake motions. Bull Earthquake Res Inst 39:85–95

Kennedy J, Eberhart R (1995) Particle swarm optimization. In: Proceedings of IEEE International Conference on Neural Networks. Perth, Australia, pp 1942–1948

Khashaee P, Mohraz B, Sadek F et al (2003) Distribution of earthquake input energy in structures. National Institute of Standards and Technology, Gaithersburg

Khatibinia M, Yazdani H (2018) Accelerated multi-gravitational search algorithm for size optimization of truss structures. Swarm Evol Comput 38:109–119. https://doi.org/10.1016/j.swevo.2017.07.001

Khatibinia M, Gholami H, Labbafi SF (2016) Multi–objective optimization of tuned mass dampers considering soil–structure interaction. Int J Optim Civil Eng 6:595–610

Khatibinia M, Gholami H, Kamgar R (2017) Optimal design of tuned mass dampers subjected to continuous stationary critical excitation. Int J Dyn Control:1–11. https://doi.org/10.1007/s40435-017-0386-7

Kuwamura H, Galambos TV (1989) Earthquake load for structural reliability. J Struct Eng 115:1446–1462. https://doi.org/10.1061/(ASCE)0733-9445(1989)115:6(1446)

Leung AYT, Zhang H (2009) Particle swarm optimization of tuned mass dampers. Eng Struct 31:715–728. https://doi.org/10.1016/j.engstruct.2008.11.017

Leung AYT, Zhang H, Cheng CC, Lee YY (2008) Particle swarm optimization of TMD by non-stationary base excitation during earthquake. Earthq Eng Struct Dyn 37:1223–1246. https://doi.org/10.1002/eqe.811

Lignos, D. G., and Krawinkler, H. (2011) Deterioration modeling of steel components in support of collapse prediction of steel moment frames under earthquake loading, J. Struct. Eng. 137(11): 1291-302.

Lu Z, Li K, Ouyang Y, Shan J (2018) Performance-based optimal design of tuned impact damper for seismically excited nonlinear building. Eng Struct 160:314–327. https://doi.org/10.1016/j.engstruct.2018.01.042

Mazzoni S, Mckenna F, Scott MH, Fenves GL (2006) The open system for earthquake engineering simulation (OpenSEES) user command-language manual

Mohebbi M, Joghataie A (2012) Designing optimal tuned mass dampers for nonlinear frames by distributed genetic algorithms. Struct Design Tall Spec Build 21:57–76. https://doi.org/10.1002/tal.702

Mokarram V, Banan MR (2018) A new PSO-based algorithm for multi-objective optimization with continuous and discrete design variables. Struct Multidiscip Optim 57:509–533. https://doi.org/10.1007/s00158-017-1764-7

Nigdeli SM, Bekdas G (2013) Optimum tuned mass damper design for preventing brittle fracture of RC buildings. Smart Struct Syst 12:137–155. https://doi.org/10.12989/sss.2013.12.2.137

Nigdeli SM, Bekdaş G, Sayin B (2017) Optimum tuned mass damper design using harmony search with comparison of classical methods. AIP Conf Proc 1863:540004. https://doi.org/10.1063/1.4992681

Rana R, Soong TT (1998) Parametric study and simplified design of tuned mass dampers. Eng Struct 20:193–204. https://doi.org/10.1016/S0141-0296(97)00078-3

Saaed TE, Nikolakopoulos G, Jonasson J-E, Hedlund H (2015) A state-of-the-art review of structural control systems. J Vib Control 21:919–937. https://doi.org/10.1177/1077546313478294

Sadek F, Mohraz B, Taylor AW, Chung RM (1997) A method of estimating the parameters of tuned mass dampers for seismic applications. Earthq Eng Struct Dyn 26:617–635. https://doi.org/10.1002/(SICI)1096-9845(199706)26:6<617::AID-EQE664>3.0.CO;2-Z

Shahrouzi M, Nouri G, Salehi N (2017) Optimal seismic control of steel bridges by single and multiple tuned mass dampers using charged system search. Int J Civ Eng 15:309–318. https://doi.org/10.1007/s40999-016-0102-6

Shi Y, Eberhart R (1998) A modified particle swarm optimizer. In: 1998 IEEE International Conference on Evolutionary Computation

Proceedings. IEEE World Congress on Computational Intelligence (Cat. No.98TH8360), pp 69–73

Singh MP, Moreschi LM (2002) Optimal placement of dampers for passive response control. Earthq Eng Struct Dyn 31:955–976. https://doi.org/10.1002/eqe.132

Singh MP, Singh S, Moreschi LM (2002) Tuned mass dampers for response control of torsional buildings. Earthq Eng Struct Dyn 31: 749–769. https://doi.org/10.1002/eqe.119

Tajimi H (1960) Statistical method of determining the maximum response of a building structure during an earthquake. In: Proceedings of the 2nd World Conference on Earthquake Engineering. Tokyo, Japan, pp 781–798

Villaverde R (1985) Reduction seismic response with heavily-damped vibration absorbers. Earthq Eng Struct Dyn 13:33–42. https://doi.org/10.1002/eqe.4290130105

Warburton GB (1982) Optimum absorber parameters for various combinations of response and excitation parameters. Earthq Eng Struct Dyn 10:381–401. https://doi.org/10.1002/eqe.4290100304

Wirsching PH, Campbell GW (1973) Minimal structural response under random excitation using the vibration absorber. Earthq Eng Struct Dyn 2:303–312. https://doi.org/10.1002/eqe.4290020402

Wirsching PH, Yao JTP (1973) Safety design concepts for seismic structures. Comput Struct 3:809–826. https://doi.org/10.1016/0045-7949(73)90060-6

Wong KK (2008) Seismic energy dissipation of inelastic structures with tuned mass dampers. J Eng Mech 134:163–172. https://doi.org/10.1061/(ASCE)0733-9399(2008)134:2(163)

Wong KK, Harris JL (2010) Seismic damage and fragility analysis of structures with tuned mass dampers based on plastic energy. Struct Design Tall Spec Build 21:296–310. https://doi.org/10.1002/tal.604

Wu J, Chen G, Lou M (1999) Seismic effectiveness of tuned mass dampers considering soil–structure interaction. Earthq Eng Struct Dyn 28:1219–1233. https://doi.org/10.1002/(SICI)1096-9845(199911)28:11<1219::AID-EQE861>3.0.CO;2-G

Yazdani H, Khatibinia M, Gharehbaghi S, Hatami K (2017) Probabilistic performance-based optimum seismic design of RC structures considering soil–structure interaction effects. ASCE-ASME J risk uncertain. Eng Syst Part Civ Eng 3:G4016004. https://doi.org/10.1061/AJRUA6.0000880

Zhang HY, Zhang LJ (2017) Tuned mass damper system of high-rise intake towers optimized by improved harmony search algorithm. Eng Struct 138:270–282. https://doi.org/10.1016/j.engstruct.2017.02.011